

Generalised Fourier Series Model for Dual Active Bridge DC/DC Converter based on Triple Phase Shift Modulation Method

M. I. Rahman
School of Engineering
University of Aberdeen
Aberdeen, UK

D. Jovcic
School of Engineering
University of Aberdeen
Aberdeen, UK

K. H. Ahmed
Department of Electronic and Electrical
Engineering
University of Strathclyde
Glasgow, UK

Abstract—This paper presents a generic model for the dual active bridge DC/DC converter. The model is based on the Fourier series of the switching functions of the converter. The switching functions are firstly derived with all the possible control variables identified for the converter. The triple phase shift modulation control method is realised for this work. Other modulation methods such as the phase shift control, dual phase shift control and pulse-width modulation control can be derived from the triple phase shift control model. The dynamic harmonic model of the DC capacitor voltages, DC currents, AC voltages and the AC inductor current are derived. The harmonic model is verified using MATLAB/Simulink software to match the derived model with a detailed switched model of the dual active bridge DC/DC converter. Further, a 500 W 24/100 V prototype is built to confirm the work.

Index Terms—Dual active bridge (DAB), DAB model, Harmonic model, Triple phase shift, Generalised model

I. INTRODUCTION

The Dual Active Bridge (DAB) DC/DC converter is one of the important components that can facilitate the development of high power DC grids [1]-[2]. A model is required to analyse the converter performance, design optimisation and controller development, however it is known that DC-DC modelling impose numerous challenges [2]-[7].

Most of the developed models consist of steady-state and small signal model [3]-[7]. The steady-state model is used to determine different parameters such as the series inductance design [3], [6] and the small signal model predicts the dynamic of the DAB converter, which is important for controller development, and transient analysis [4], [7]. Differential equations are normally used for time domain analysis which are time varying and nonlinear. The converter model can be derived using 1) State-space averaging method, or 2) Fundamental harmonic approximation (FHA) method.

The DAB model that uses state space averaging method is reported in [2], [3], [8] because of the symmetrical structure of the DAB, that can be averaged over the switching cycle. The operation of the DAB converter is describe based on piecewise sequence of the inductor current where it is split into triangular or trapezoidal shapes over the switching cycle [9]-[11]. Average model based on different control methods such as phase shift (PS), extended phase shift (EPS), dual phase shift (DPS), triple phase shift (TPS) and duty cycle modulation are available in [3], [5]-[6], [9], [11]. However, the derived state-space averaging equations in the literature are specific for a control method and operation. The derivation of the equations from state-space averaging

method can become exponentially complex as additional degrees of freedom are to be included if other control methods are considered. It can also lead to complicated matrix that is more difficult to solve and analyse.

FHA is a common approach to describe the large and small signal behaviour of power electronic systems [1], [5], [12] which is simpler and easy to use. The simplification of the FHA method considering only the first harmonic component of the square wave AC voltages can lead to all the converter variables to be expressed by its magnitude and phase (AC phasor theory) [5]-[6]. The voltage magnitude is slightly lower in FHA as higher harmonics are neglected. Therefore, higher harmonics component needs to be included to accurately model the converter. Mathematical model for various operating conditions, optimisation of reactive current, and DC fault studies are reported in [6], [13]-[14], however they are based on its fundamental frequency.

Most cited papers present a model which is valid for specific control methods or operation modes. The modelling technique utilise in this paper is the harmonic approximation to derive the trigonometric expressions of the DAB converter AC voltages, AC inductor current, DC capacitor voltages, and DC currents. Fourier series expansion is used in modelling the dynamic equation to accurately indicate the converter operation during steady-state and transient. The aim of the study is to develop static, parametric model of the converter so that it can be used for different control modulation method by considering all the control signals identified in the literature. A 3 MW 4/40 kV DAB DC/DC converter modelled in MATLAB/Simulink is used to compare and validate the equation derived. A DAB prototype rated at 500 W 24/100 V is realised to validate the work.

II. DUAL ACTIVE BRIDGE DC/DC CONVERTER TOPOLOGY

A. Basic Operation

The DAB converter is shown in Fig. 1. The principle of operation is described based on the widely used PS control method [1], [5].

$$i_{cdc1}(t) = C_{dc1} \frac{d(V_{dc1}(t) - V_{R_{dc1}}(t))}{dt} = C_{dc1} \frac{dV_{Cdc1}(t)}{dt} \quad (4)$$

$$i_{cdc2}(t) = C_{dc2} \frac{d(V_{dc2}(t) - V_{R_{dc2}}(t))}{dt} = C_{dc2} \frac{dV_{Cdc2}(t)}{dt} \quad (5)$$

where $V_{dc1}(t)$ is the LV side DC terminal voltage, $V_{dc2}(t)$ is the HV side DC terminal voltage, $V_{R_{dc1}}(t) = i_1(t)R_{dc1}$ is the voltage across the DC resistance, R_{dc1} , $V_{R_{dc2}}(t) = i_2(t)R_{dc2}$ is the voltage across the DC resistance, R_{dc2} , and the voltages across the DC capacitor, $V_{Cdc1}(t)$ and $V_{Cdc2}(t)$. This DC capacitor voltage can be assumed similar to the DC terminal voltages, $V_{dc1}(t)$ and $V_{dc2}(t)$ if the voltage drop across the DC resistances, R_{dc1} and R_{dc2} are small. The DC side currents can be determined as

$$i_1(t) = i_{cdc1}(t) + i_{dc1}(t) \quad (6)$$

$$i_2(t) = -i_{cdc2}(t) + i_{dc2}(t) \quad (7)$$

where $i_1(t)$ and $i_2(t)$ are the DC terminal currents in LV and HV sides, respectively, $i_{dc1}(t)$ is the current flowing through LV side bridge and $i_{dc2}(t)$ is the current coming out from HV side bridge. The currents $i_{dc1}(t)$ and $i_{dc2}(t)$ depend on the instantaneous inductor current, i_L . Therefore, the currents $i_{dc1}(t)$ and $i_{dc2}(t)$ can only flow when the switch states are non-zero. These $i_{dc1}(t)$ and $i_{dc2}(t)$ are require derivation but $i_1(t)$ and $i_2(t)$ can be easily determined since they are measurable signals.

B. AC subsystem

As the dynamic of the DC sides of the DAB are modelled, the time domain equation for AC subsystem of the converter shall be determined based on the AC equivalent circuit of the converter as in Fig. 3.

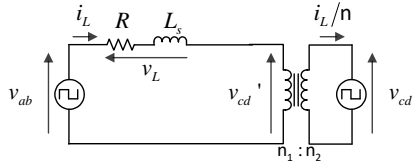


Fig. 3: AC side subsystem DAB equivalent circuit (square wave voltages)

The transformer parameters such as the windings, leakage inductances are assumed to be very small and magnetizing component of the transformer is large enough to not affect the converter operation. Therefore, the series inductance, L_s dominates the inductance of the converter. For simplifying analysis, the transformer is simplified by referring the model to one side. The inductor voltage, $v_L(t)$ can be expressed as

$$v_L(t) = L_s \frac{di_L(t)}{dt} + Ri_L(t) = v_{ab}(t) - v_{cd}'(t) \quad (8)$$

With the basic dynamic model derived for both DC and AC sides subsystem, the DAB converter harmonic modelling based on Fourier series is shown in the following section.

IV. HARMONIC MODELLING OF THE DAB CONVERTER

The square wave AC voltages of the DAB converter can be represented by infinite number of sinusoids functions using Fourier series [7]. The converter bridge switched the

DC terminal voltage source into square wave functions which contain only odd harmonics. According to the Fourier transformation, the maximum value of the first harmonic of a square wave is $(4/\pi)$ times of the maximum value of the square wave signal.

A. AC voltages

The DAB converter generates square wave AC voltages. Therefore, the AC voltage variables on each leg can be expressed in terms of its harmonics to create a highly accurate DAB converter model. The AC voltages $v_{an}(t)$ and $v_{cn}(t)$ are:

$$v_{an}(t) = \frac{2V_{dc1}}{\pi} \sin\left(\frac{\gamma_1}{2}\right) \sum_{n=1}^N \left(\frac{\sin((2n-1)(\omega t - \beta_1 - \alpha_1))}{(2n-1)} \right) \quad (9)$$

$$v_{cn}(t) = \frac{2V_{dc2}}{\pi} \sin\left(\frac{\gamma_2}{2}\right) \sum_{n=1}^N \left(\frac{\sin((2n-1)(\omega t - \beta_2 - \alpha_2))}{(2n-1)} \right) \quad (10)$$

The voltage equations in (1) and (2) can be expressed in terms of (9) to (10), $v_{bn}(t) = -v_{an}(t)$ and $v_{dn}(t) = -v_{cn}(t)$ as in (A1) and (A2). Equations (A1) and (A2) in the Appendix are the general AC voltage equations at LV side and HV side (referred to LV side), respectively. It can be used to analyse PS, EPS, DPS, TPS and PWM-PS control following the assumptions in [18]. The following section expresses the harmonic equation based on the AC voltage harmonic model.

B. AC Inductor current

The AC inductor current can now be represented using the derived AC voltages by substituting (A1) and (A2) to (8). Due to the nature of differential equation in (8), it is difficult to express the converter AC inductor current. Since the converter is operating at fixed frequency and for ease of analysing the converter current, AC phasor analysis is used to represent individual harmonics of the inductor current based on its magnitude and phase. The derivative term in (8) can be replaced with its frequency domain ($j\omega$). Expression of the left hand term and right hand term in (8) are available in [18]. From this, the inductor current equation in time domain can be expressed as in (A3) of the Appendix where it can be used to express the generic AC inductor current of the DAB converter.

C. DC currents

With the AC inductor current expression in (A3), the DC side currents can be substituted conveniently because the AC inductor current is expressed by the switching of the AC voltages. Therefore, the AC inductor current and AC voltages can be related to the DC side currents, $i_{dc1}(t)$ and $i_{dc2}(t)$. Assuming the power at DC side is equal to the power at AC side,

$$P_{dc1}(t) = P_{ac1}(t) \quad (11)$$

$$V_{dc1}(t)i_{dc1}(t) = \text{real}(v_{ab}(t)i_L(t)^*)$$

where the LHS of (11) is the DC power equation and the RHS of (11) gives the AC power equation. RMS voltage and current shall be used for the AC power variables and therefore becomes

$$V_{dc1}(t)i_{dc1}(t) = \frac{1}{2}(\text{real}(v_{ab}(t)i_L(t)^*)) \quad (12)$$

The DC current, $i_{dc1}(t)$ in (12) is the input of the DAB converter model and the DC terminal voltage, $V_{dc1}(t)$ is constant. The HV DC current can be expressed similarly using (11) and (12). The DC-AC power balance equation in (12) is used to link the DC and AC current as (13).

$$i_{dc1}(t) = \frac{\text{real}(v_{ab}(t)i_L(t)^*)}{2V_{dc1}(t)} = \frac{\text{real}((v_{an}(t) - v_{bn}(t))i_L(t)^*)}{2V_{dc1}(t)} \quad (13)$$

The $i_{dc1}(t)$ in (13) is similar to $i_{dc2}(t)$. Equations (9) to (10) and (A3) can be substituted into (13) to give the full DC currents terms as available in [18]. The general equations for the DC side currents are still complex because of the DC and AC harmonics content. Simplification is made by following the power balance equation where it gives link between the harmonics of the AC and DC variables by taking its similarities.

D. DC capacitor currents and voltages

The DC capacitor current, $i_{cdc1}(t)$ and $i_{cdc2}(t)$ can be expressed as

$$i_{cdc1}(t) = i_1(t) - i_{dc1}(t) \quad (14)$$

$$i_{cdc2}(t) = -i_2(t) + i_{dc2}(t) \quad (15)$$

Equations (14) and (15) can be substituted with the DC currents derived in (13) as available in [18]. The LV and HV side DC capacitor voltages in time domain can be substituted using the DC capacitor currents. The DC capacitor voltage differential equations can be rewritten from (4) and (5). The dynamic equations of the DAB converter has been derived successfully based on its harmonic components that can be employed for different control methods.

V. HARMONIC MODEL VERIFICATION

The harmonic model is simulated in MATLAB to match the DAB converter switched model developed in MATLAB/Simulink. The DAB converter specification is given in Table I and the full TPS control harmonic model is depicted in Fig. 4. Since the Fourier series have unlimited summation of harmonics, it is known that the more harmonics component are included, the more accurate the matching of the waveform. Therefore, it is important to determine the number of harmonics to be included. Based on the preliminary simulation, considering the first five harmonics in the model ($n = 5$) gives better representation of the signal (difference is about 0.014% from the original signal). If more harmonics are to be included, the difference becomes negligible. Hence, n-th harmonic of five is chosen for the verification of the dynamic model for all the control modulation methods. For the following simulations, the monitored variables are the AC voltage equations, $v_{ab}(t)$, $v_{cd}(t)$ in (A1), (A2), inductor current, $i_L(t)$ in (A3) and DC current, $i_{dc1}(t)$. Only LV DC current is shown because the characteristics are similar. The DC capacitor voltages are not shown because of the nature of the application where the DC capacitor voltages are closely tied with the DC terminal voltage of the DAB converter. However, (4) and (5) can be

rewritten and used to obtain the DC capacitor voltage for the intended user application such as energy storage system.

A. Steady-state verification

In this section, only the verification of TPS control is shown. Fig. 5 gives the AC sides variables (AC voltages and inductor current) and the DC sides currents which are

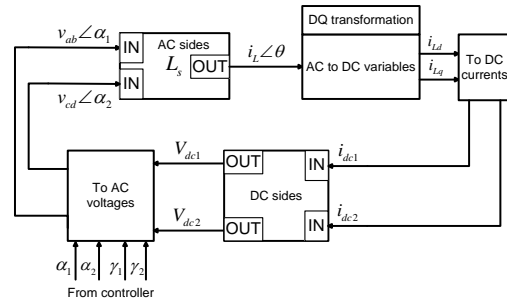


Fig. 4: DAB DC/DC converter Harmonic model

compare with the switched model. Maximum PS angle of 90° is chosen with the inner PS at LV side bridge, β_2 is set at 30° and inner PS at HV side bridge, β_4 is set at 60° . It can be observed that the derived dynamic model is able to match the variables of the switched model in MATLAB/Simulink.

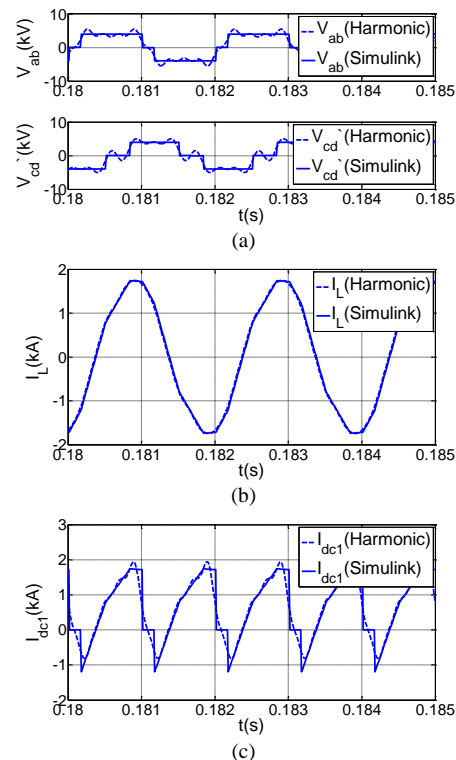


Fig. 5: Triple phase shift control AC sides waveforms (a) AC voltages, (b) AC inductor current, and (c) LV DC current

B. Step-input verification

A small-signal perturbation is investigated to verify the dynamic model response against input variations. Changes to the inductor current and DC current variables are expected when a small step input is applied to a) The PS angle, α_2 to varied the power level, and b) The LV side DC voltage is reduced to zero.

TABLE I: SYSTEM PARAMETERS AT RATED POWER

Parameters	Value
------------	-------

Power, P_1	3 MW
DC voltage at LV, V_{dc1}	4 kV
DC voltage at HV, V_{dc2}	40 kV
Fundamental RMS AC voltage at LV, v_{ac1}	3.6 kV
Fundamental RMS AC voltage at HV, v_{ac2}	36 kV
Average DC current at LV, I_{dc1}	750 A
Average DC current at HV, I_{dc2}	75 A
Fundamental RMS AC current at LV, $I_{Lm LV}$	1200 A
Fundamental RMS AC current at HV, $I_{Lm HV}$	120 A
Operating frequency, f	500 Hz

The first verification is to apply step input to the PS angle of the harmonic model and the switched model. The initial PS angle is set at 90° and then a small step to the PS angle is applied at 88.5 ms to 75° . It is observed in Fig. 6(a) that the AC voltages on the HV side has changed slightly to the left (the difference between the LV and HV sides AC voltages is smaller). The inductor current, i_L is expected to decrease when PS angle decreases as verified in Fig. 6(b). The small step also affects the DC side current variable, i_{dc1} as in Fig. 6(c). Although the harmonic model follows the step changes, the transient time of the harmonic model and MATLAB/Simulink modelled are different. Further tests with different the inner PS angles have given similar accurate results such.

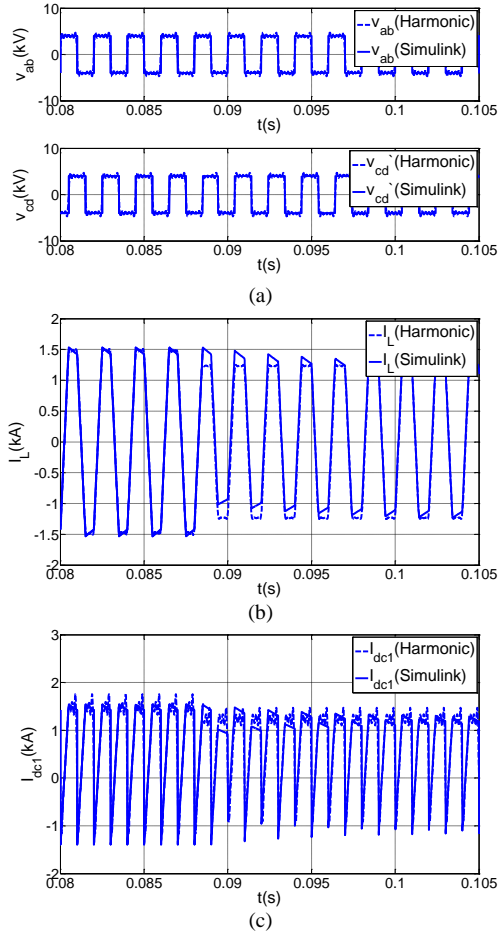


Fig. 6: The AC sides waveforms when step is applied to the PS angle, α_2 (from 90° to 75°), (a) AC voltages, (b) AC inductor current, and (c) LV DC current

The second verification test is to apply step input to the DC voltages of the harmonic model and the switched model. The selected DC terminal for this verification is the LV side. The LV side is simulated to have DC fault at 88.5 ms. The LV DC side is initially operating at 4 kV down to 0 V (fault is

applied). It is observed in Fig. 7(a) that the AC voltage on the LV side changes to zero value and the harmonic model is able to follow the DAB switched model. The inductor current, i_L and DC current waveform, i_{dc1} characteristics are as expected as in the literature on DC fault available in [14].

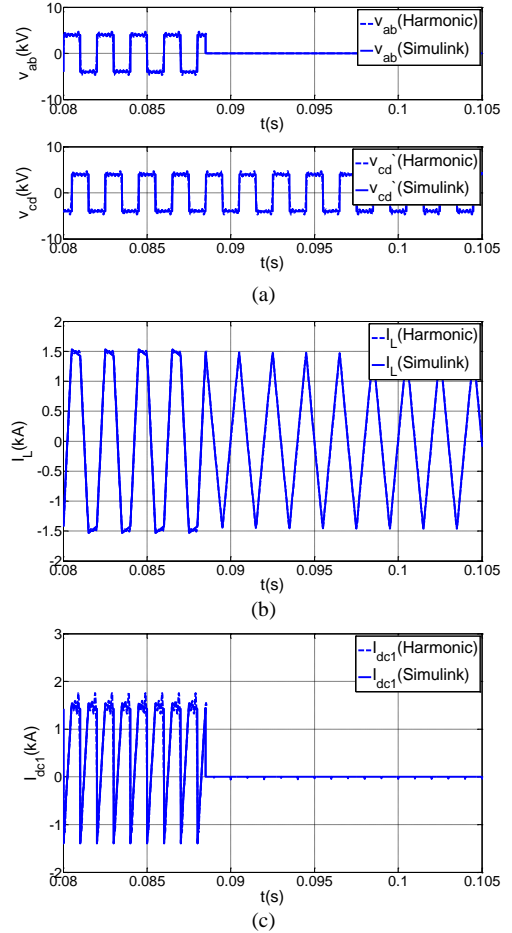


Fig. 7: The AC sides waveforms when step is applied to the LV DC side terminal from 4 kV to 0 kV (Fault is applied), (a) AC voltages, (b) AC inductor current, and (c) LV DC current

This step input response further verifies that the harmonic model developed in this paper is able to follow the changes applied to the PS angle and DC terminal voltage.

VI. PROTOTYPE VERIFICATION

Fig. 8 shows the DAB DC/DC converter prototype built to validate this work. The specification of the converter is 500 W, 24 / 100 V operating at 2000 Hz.

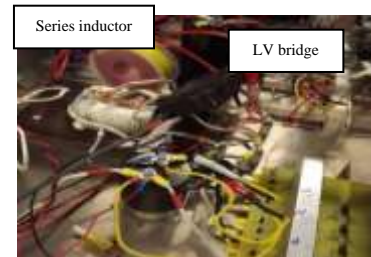


Fig. 8. DAB DC/DC converter 500 W prototype

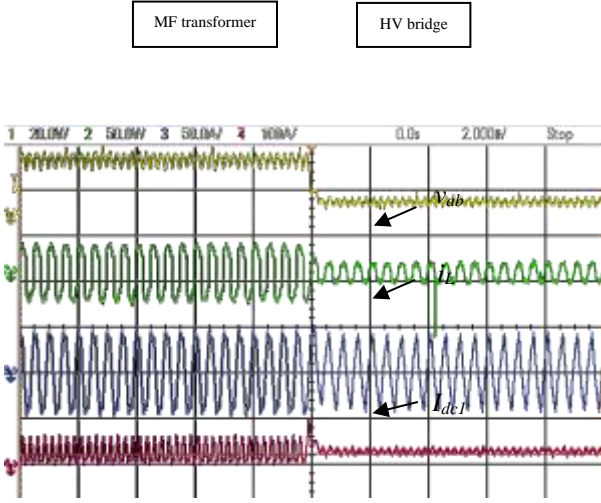


Fig. 9. Practical results at LV DC fault

Only the work when DC fault is applied at LV side is validated. The practical waveforms of the converter during DC fault are shown in Fig. 9. It is observed that the waveforms of v_{ab} , i_L and I_{dc1} shows satisfactory matched with the harmonic model and simulated results in Fig. 7.

VII. CONCLUSION

The derived DAB converter dynamic model is based on the harmonics approximation method (only up to the 5-th harmonic is considered for validation) is used to describe the converter behaviour change over time. The converter AC inductor current, AC voltages, DC side currents and DC side capacitor voltages are derived. The harmonic model is validated by comparing with the switched detailed model developed in MATLAB/Simulink. Verification is done for steady-state and small step input is applied to the PS angle, inner PS angle and DC terminal voltage. The verification when DC fault is applied to the LV side DC terminal is practically validated. The harmonic model can predict the DAB variables operating waveforms with minimal errors are observed.

REFERENCES

[1] D. Jovcic and H. Zhang, "Dual Channel Control with DC Fault Ride Through for MMC-based, Isolated DC/DC Converter" *IEEE Trans. Power Delivery.*, vol. 32, no. 3, pp. 1574-1582, June 2017.

[2] W Lin and D Jovcic, "Average modelling of medium frequency DC/DC converters in dynamic studies" *IEEE Trans. Power Delivery*, vol. 30, no. 1, pp 281-289, Jan. 2015.

[3] A. Tong, L. Hang, G. Li, X. Jiang and S. Gao, "Modeling and Analysis of a Dual-Active-Bridge-Isolated Bidirectional DC/DC Converter to Minimize RMS Current With Whole Operating Range," *IEEE Trans. Power Electron.*, vol. 33, no. 6, pp. 5302-5316, June 2018.

[4] H. Qin, and J.W. Kimball, "Generalized average modelling of dual active bridge dc-dc converter," *IEEE Trans. Power Electron.*, vol. 27, no. 4, pp. 2078-2084, April 2012.

[5] S.S. Shah and S. Bhattacharya, "A Simple Unified Model for Generic Operation of Dual Active Bridge Converter," *IEEE Trans. Ind. Electron.*, vol. 66, no. 5, pp. 3486-3495, May 2019.

[6] M.I. Rahman, D. Jovcic, and K.H. Ahmed, "Reactive current optimisation for high power dual active bridge dc/dc converter," *Proc. IEEE PowerTech*, Grenoble, 2013, pp. 1-6.

[7] H. Bai, C. Mi, C. Wang, and S. Gargies, "The dynamic model and hybrid phase-shift control of a dual-active-bridge converter," *Proc. IEEE Ind. Electron.*, Orlando, FL, 2008, pp. 2840-2845.

[8] J.A. Mueller and J.W. Kimball, "Modeling Dual Active Bridge Converters in DC Distribution Systems," *IEEE Trans. Power Electron.*, vol. 34, no. 6, pp. 5867-5879, June 2019.

[9] Y.A. Harrye, K.H. Ahmed, G.P. Adam, and A.A. Aboushady, "Comprehensive steady state analysis of bidirectional dual active bridge dc/dc converter using triple phase shift control," *Proc. Ind. Electron.*, Istanbul, 2014, pp. 437-442.

[10] H. Bai, C. Mi, and S. Gargies, "The short-time-scale transient processes in high-voltage and high-power isolated bidirectional dc-dc converters," *IEEE Trans. Power Electron.*, vol. 23, no. 6, pp. 2648-2656, Nov. 2008.

[11] G.D. Demetriades, and H.P. Nee, "Characterization of the dual-active bridge topology for high-power applications employing a duty-cycle modulation," *Proc. IEEE Power Electron. Specialists Conf.*, Rhodes, 2008, pp. 2791-2798.

[12] R.W. De Doncker, D.M. Divan, and M.H. Kheraluwala, "A three-phase soft-switched high-power-density dc/dc converter for high power applications," *IEEE Trans. Ind. Appl.*, vol. 27, no. 1, pp. 63-73, Jan/Feb. 1991.

[13] R.P. Twiname, D.J. Thrimawithana, U.K. Madawala, and C.A. Baguley, "A new resonant bi-directional dc-dc converter topology," *IEEE Trans. Power Electron.*, vol. 29, no. 9, pp. 4733-4740, Sept. 2014.

[14] M.I. Rahman, K. H. Ahmed and D. Jovcic, "Analysis of DC Fault for Dual-Active Bridge DC/DC Converter Including Prototype Verification," *IEEE Journal of Emerging and Selected Topics in Power Electron.*, vol. 7, no. 2, pp. 1107-1115, June 2019.

[15] B. Zhao, Q. Yu, and W. Sun, "Extended-phase-shift control of isolated bidirectional dc-dc converter for power distribution in microgrid," *IEEE Trans. Power Electron.*, vol. 27, no. 11, pp. 4667-4680, Nov. 2012.

[16] A.K. Jain, and R. Ayyanar, "PWM control of dual active bridge: Comprehensive analysis and experimental verification," *IEEE Trans. Power Electron.*, vol. 26, no. 4, pp. 1215-1227, April 2011.

[17] D. Kanase, "Comparative Study of Feed Forward and SPWM Control Technique for DC to DC Dual Active Bridge Converter Driving Single Phase Inverter," *Int. Journal for Innovative Research in Science & Tech.*, 3, 2016.

[18] M.I. Rahman, "Dual Active Bridge DC/DC converter with internal transformer for high power applications," Ph.D. dissertation, School of Engineering, University of Aberdeen, UK, 2020.

APPENDIX

$$v_{ab}(t) = \frac{2V_{dc1}}{\pi} \sin\left(\frac{\gamma_1}{2}\right) \sum_{n=1}^N \left(\frac{\sin((2n-1)\omega t)}{(2n-1)} \right) + \frac{2V_{dc1}}{\pi} \sin\left(\frac{\gamma_1}{2}\right) \sum_{n=1}^N \left(\frac{\sin((2n-1)(\omega t - \beta_2))}{(2n-1)} \right) \quad (A1)$$

$$v_{cd}(t) = \frac{2V_{dc2}}{\pi} \sin\left(\frac{\gamma_2}{2}\right) \sum_{n=1}^N \left(\frac{\sin((2n-1)(\omega t - \alpha_2))}{(2n-1)} \right) + \frac{2V_{dc2}}{\pi} \sin\left(\frac{\gamma_2}{2}\right) \sum_{n=1}^N \left(\frac{\sin((2n-1)(\omega t - \beta_4 - \alpha_2))}{(2n-1)} \right) \quad (A2)$$

$$i_L(t) = \left(\frac{2V_{dc1}}{\pi} \sin\left(\frac{\gamma_1}{2}\right) \sum_{n=1}^N \left(\frac{\sin((2n-1)\omega t - \theta_c(n))}{(2n-1)|Z(n)|} \right) \right) - \left(\frac{2V_{dc2}}{\pi} \sin\left(\frac{\gamma_2}{2}\right) \sum_{n=1}^N \left(\frac{\sin((2n-1)(\omega t - \alpha_2) - \theta_c(n))}{(2n-1)|Z(n)|} \right) \right) + \left(\frac{2V_{dc1}}{\pi} \sin\left(\frac{\gamma_1}{2}\right) \sum_{n=1}^N \left(\frac{\sin((2n-1)(\omega t - \beta_2) - \theta_c(n))}{(2n-1)|Z(n)|} \right) \right) - \left(\frac{2V_{dc2}}{\pi} \sin\left(\frac{\gamma_2}{2}\right) \sum_{n=1}^N \left(\frac{\sin((2n-1)(\omega t - \beta_4 - \alpha_2) - \theta_c(n))}{(2n-1)|Z(n)|} \right) \right) \quad (A3)$$